Journal of Materials Chemistry

Cite this: *J. Mater. Chem.*, 2011, **21**, 11916

www.rsc.org/materials

PAPER

A hybrid material of vanadium nitride and nitrogen-doped graphene for lithium storage†

Kejun Zhang,‡[a] Haibo Wang,‡[a] Xiaoqing He,‡[b] Zhihong Liu,[a] Li Wang,[ac] Lin Gu,*[b] Hongxia Xu,[a] Pengxian Han,[a] Shanmu Dong,[a] Chuanjian Zhang,[a] Jianhua Yao,[a] Guanglei Cui*[a] and Liquan Chen[b]

Received 20th April 2011, Accepted 3rd June 2011
DOI: 10.1039/c1jm11710f

Vanadium nitride and nitrogen-doped graphene nanosheet (G) hybrid materials were prepared by a facile sol–gel method combined with a thermal treatment at 800 °C under ammonia atmosphere. It was found that VN nanoparticles adhered to the surface of nitrogen-doped graphene nanosheets and/or were embedded in the graphene layers of the hybrid material (VN-G). This nanostructured material promises an efficient electronic and ionic conducting network, which exhibits dramatically increased specific capacities after rate capability test in comparison to the original value under the same current density. The most probable explanations for these distinct characteristics are deduced from observations by advanced transmission electron microscopy together with X-ray diffraction and electron energy-loss spectroscopy, which illustrate a gradual activation of nitride during lithiation/delithiation processes, owing to slow kinetics of VN reaction with lithium. The electrochemical results demonstrate that the weight ratio of VN to G has a significant effect on the performance and related kinetics of the materials.

1. Introduction

Rechargeable lithium-ion batteries have long been considered an attractive power source for a wide variety of applications over traditional rechargeable battery systems.[1–4] Carbonaceous materials are most commonly used as anode materials in today's lithium ion batteries. With the growing demand for high energy density secondary batteries, the low capacity of graphite (theoretical capacity: 372 mAh g^{-1}) has become limited for a wider applications. At present, novel anode materials and the related mechanism are extensively explored to improve capacity performance and rate capability.[5–10]

Vanadium nitride (VN) material possesses the advantages of corrosion resistance, high temperature and chemical stability.[11] It was reported that VN thin film exhibited a higher discharge capacity of 1500 mAh g^{-1} despite a tedious and expensive magnetron sputtering method.[12] Therefore, VN is anticipated to show a potential application in high energy anode material. However, VN nanoparticles were reported to exhibit a poor electronic conductivity at room temperature, which might result in limited rate capability.[13]

Graphene, a two dimensional form of carbon,[14] promises a wide range of technological applications, such as supercapacitors,[15] hydrogen storage[16] and lithium ion batteries[17] owing to advantages in terms of its electronic, thermal, mechanical strength, physicochemical properties.[18–23] Some attempts have also been made to use graphene as support and electronic materials to improve their lithium storage behavior.[24–26] Recently, nitrogen-doped graphene nanosheets (G) were obtained by thermal annealing of graphite oxide (GO) in NH_3 atmosphere, which shows better electrochemical performance than pristine graphene.[27] Inspired by the above successful examples, we designed vanadium nitride and nitrogen-doped graphene nanosheets (VN-G), which could be expected to deliver the ingredients for more efficient charge transportation and storage.

Herein, we presented a simple sol–gel process followed by ammonia annealing for preparation of a series of VN-G hybrid materials. The electrochemical properties of these series samples have been investigated in detail. Interestingly, it was also found that all the hybrid showed dramatically increasing specific capacities after rate tests or extended cycling when compared with the original value under the same current density. The related mechanism was explored based on monitoring structural changes after cycling using EELS, TEM and XRD.

[a]*Qingdao Institute of Bioenergy and Bioprocess Technology, Chinese Academy of Sciences, Qingdao, 266101, P.R. China. E-mail: cuigl@qibebt.ac.cn; l.gu@iphy.ac.cn; Fax: +86 532 80662744; Tel: +86 532 80662746*
[b]*Beijing National Laboratory for Condensed Matter Physics, The Institute of Physics, Chinese Academy of Sciences, Beijing, 100190, China*
[c]*Ocean University of China, Qingdao, 266003, P.R.China*
† Electronic supplementary information (ESI) available: Supplementary information. See DOI: 10.1039/c1jm11710f
‡ These authors contributed to the work equally.

2. Experimental

2.1 Preparation of samples

Vanadium pentaoxide (V_2O_5) and hydrogen peroxide (H_2O_2) were purchased from Shanghai Chemical Reagent Co. Ltd. (China). GO was prepared according to the previous literature by Hummers[28] from graphite powder (Aldrich, powder, < 20 micron, synthetic).

VN-G hybrid materials were performed by a sol–gel method (as shown in Fig. 1). 1.36 g V_2O_5 and 6 mL H_2O_2 (30%) were poured into water and a red brown solution was formed. Initial product was obtained by stirring the solution at room temperature for 1 h. Different amount of graphite oxide was added to the above $V_2O_5 \cdot nH_2O$ solution under stirring. Finally the solution was sonicated overnight to get a dark gel. The resultant $V_2O_5 \cdot nH_2O$-GO composites were dried at 80 °C for 24 h, and then calcinated at 800 °C for 5 h under an ammonia atmosphere to get VN-G hybrid. Following the same procedure, four samples denoted hereafter as VN-G-10%, VN-G-20%, VN-G-30% and VN-G-50% were prepared, which correspond to the mass ratios of VN and G are 90 : 10, 80 : 20, 70 : 30, 50 : 50, respectively. For a fair comparison, pristine VN was also prepared by the same procedure without GO.

2.2 Characterization

X-ray diffraction (XRD) of VN-G hybrid materials was recorded in a Bruker-AXS Micro-diffractometer (D8 ADVANCE) with Cu-Kα radiation (λ = 1.5406 Å) from 10 to 85°. The VN-G hybrid material, stopped at various lithiation and delithiation states, were removed from the swagelock cells in Ar-filled dry box and rinsed in anhydrous DMC (99%, Johnson Matthey) to remove residual salts. The electrodes were put in a hermetically sealed cell utilized a kapton film window for XRD measurements. A seal of silicon grease limited material contamination with air during analysis. The morphologies of VN-G samples were studied using a Hitachi S-4800 scanning electron microscope (SEM), a JEOL 2010F transmission electron microscope (TEM) and Aglient 5400 atomic force microscope (AFM), respectively. Electron energy-loss spectroscopy (EELS) was acquired using a Gatan-Imaging-Filter system attached to a Tecnai F20 microscope, which provides precise quantification of the local chemical distribution at quasi atomic scale.

2.3 Electrochemical measurements

Electrochemical performances were performed using two-electrode Swagelok type cell assembled in an argon-filled glovebox. The hybrid materials were mixed with super P and a binder poly-(vinylidene fluoride) (PVDF) at a weight ratio of 85 : 10 : 5 to form slurries. Then, the resultant slurries were uniformly pasted on Cu foil. These prepared electrode sheets were dried at 120 °C in a vacuum oven for 12 h. The electrolyte was 1.0 mol L^{-1} $LiPF_6$ in a mixture of ethylene carbonate (EC) and dimethylcarbonate (DMC) (1 : 1, v/v). Cyclic voltammetry (CV) was carried out between 3.0 and 0.01 V by employing a scan rate of 1 mV s^{-1} with IM6 electrochemical interface (Germany). The cells were charged and discharged over a voltage range of 0.01–3.0 V (*vs* Li^+/Li) at different rates and carried out with a Land battery testing system. Alternating current (AC) impedance spectra were obtained by applying a sine wave with amplitude of 5.0 mV over the frequency range from 100 kHz to 100 mHz at charge state. Fitting of the impedance spectra to the proposed equivalent circuit was performed by the code Zview.

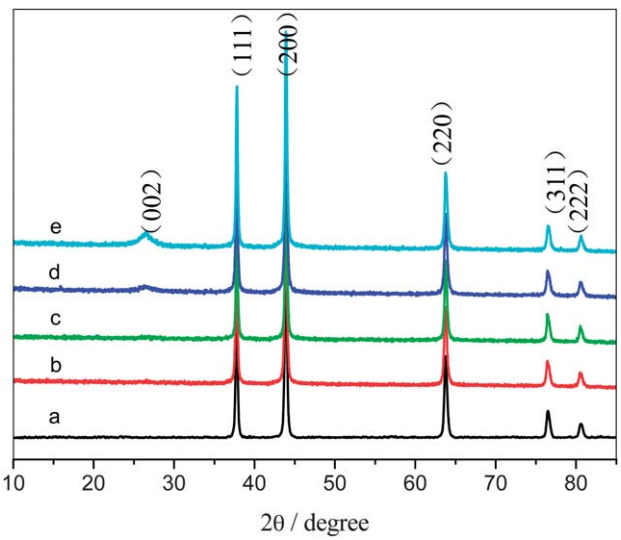

Fig. 2 XRD patterns of (a) pristine VN, (b) VN-G-10%, (c) VN-G-20%, (d) VN-G-30%, and (e) VN-G-50%.

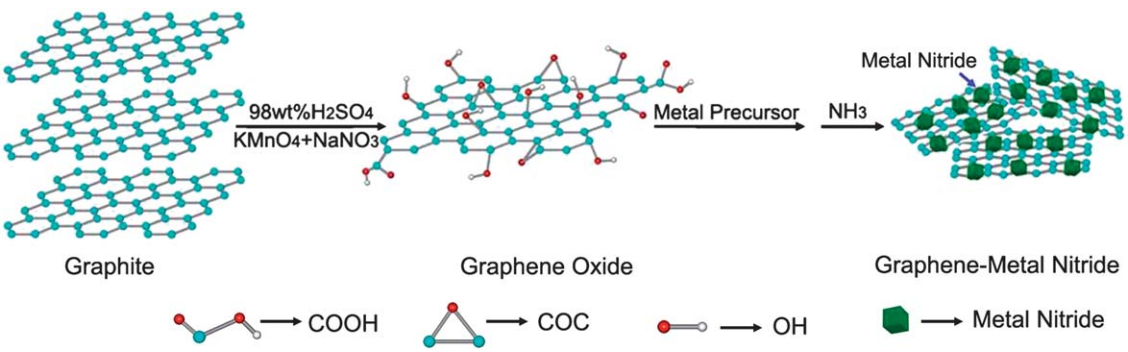

Fig. 1 A schematic illustration for preparation of VN-G hybrid materials.

3. Results and discussion

XRD patterns of the VN-G hybrid materials and pristine VN are shown in Fig. 2. The positions of diffraction peaks in the pattern are ascribed to those of cubic VN (JCPDS 73-0528).[29] The G only show a weak (002) diffraction peak at 26° (2θ) in the sample denoted as VN-G-30% and VN-G-50%, which can be indexed into the disorderedly stacked G. Moreover, with the decreasing content of VN, the broad peak becomes stronger, suggestive of more agglomeration and more stacking for G in hybrid materials.[30]

SEM images of the VN-G hybrid materials are shown in Fig. 3. It was found that the G appear corrugated into a wavy shape and the VN particles are homogenously adhered to the surface of G and/or were embedded in the G layers. Fig. 3b-e reveal that the loading amount of VN on G was effectively controlled by tuning the mass ratios of VN and G. In particular, it can be seen from Fig. 3b that G were covered by VN nanoparticles, which imply that VN nanoparticles are well electronically wired by G. Additionally, it is worth noting that the pristine VN only plates like particle were obtained if prepared without GO addition (Fig. 3a). In our method, without using surfactants and templates, VN nanoparticles adhering on G were obtained. This would ascribe to GO playing a surfactant-like role in limiting VN crystals to grow larger.[31] AFM images of VN-G-30% are shown in the supporting information Fig. S1† the thickness of G is around 3.2 nm and G is mainly multi-layer structure. A high-resolution transmission electron microscopy (HRTEM) image is shown in Fig. 3f, which illustrates two-dimensional lattice fringes of VN nanoparticles of 0.206 and 0.237 nm corresponding to the {200} and {111} lattice planes, respectively. This is consistent with the XRD measurements shown in Fig. 2.

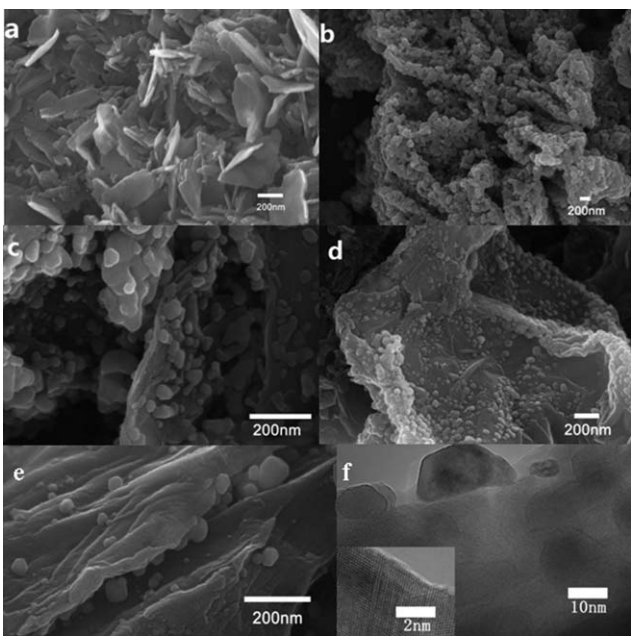

Fig. 3 SEM images of (a) pristine VN, (b) VN-G-10%, (c) VN-G-20%, (d) VN-G-30%, (e) VN-G-50% and HRTEM images of (f) VN-G-30% (inset is a high resolution image of VN particles).

Kinetics of lithium insertion/extraction in the hybrid materials can be studied using CV. The CV curves of VN-G hybrid materials and pristine VN for the initial four cycles at a scan rate of 1 mV s^{-1} are depicted in Fig. 4. In the first cycle, a small cathodic peak at 0.5 V was observed and disappeared from the second cycle in the all samples, which can be attributed to the decomposition of the electrolyte and the formation of a solid electrolyte interface (SEI).[32] A pair of redox peak at 0.01 and 0.15 V, respectively, was observed in common for the hybrid materials, which correspond to Li intercalation/de-intercalation into carbon layers.[33] After the first cycle, a couple of peaks at around 1.0 V were observed for all hybrid materials. These peaks may correspond to Li extraction/insertion reaction with the nitrides, which is common for transition metal-nitride electrodes as previously reported.[34,35]

AC impedance analysis were conducted to investigate the different resistances of the hybrid materials. As displayed in Fig. 5, a semicircle at the high to medium frequencies and a straight sloping line at low frequency can be observed. The semicircle represents charge-transfer resistance, whereas the straight sloping line is associated with diffusion resistance through the bulk of the active material. An equivalent circuit (inset of Fig. 5) was used to analyse the measured impedance data,[36] where R_e is the electrolyte resistance, and CPE_1 and R_f are the capacitance and resistance of the solid electrolyte interface (SEI) formed on the electrodes, respectively. CPE_2 and R_{ct} are the double-layer capacitance and charge-transfer resistance, respectively, Z_w is the Warburg impedance related to the diffusion of lithium ions into the bulk electrodes. The fitting values from this equivalent circuit are presented in Table 1. As can be seen, the R_f and R_{ct} of the VN electrode were 143.6 and 123.7 Ω respectively, which were significantly higher than those of the VN-G hybrid materials electrode {VN-G-10% (109.2 and 24.1 Ω), VN-G-20% (71.7 and 22.1 Ω), VN-G-30% (67.8 and 14.4 Ω), VN-G-50% (60.9 and 12.9 Ω)}. It means that both SEI resistance and charge-transfer resistance are significantly reduced in the presence of G. Moreover, it is most likely that a more favorable SEI was formed for the VN-G hybrid materials electrode than the VN, which facilitates the lithium ion transfer at the interface between the electrolyte and the electrode. This result confirmed that the graphene nanosheets not only could preserve the high conductivity of the overall electrode, but also significantly improve the electrochemical activity of metal nitride during the cycle processes.

Lithium storage properties of VN, VN-G-10%, VN-G-20%, VN-G-30% and VN-G-50% electrodes were investigated by galvanostatic discharge/charge experiments between the voltage windows of 0.01 to 3.0 V (vs Li^+/Li) in EC/DMC solution containing 1 M $LiPF_6$. As shown in Fig. 6, the current densities were increased stepwise from 21 mA g^{-1} to 2.8 A g^{-1}. The initial columbic efficiency of the VN-G-30% hybrid is 74.6%, which is much higher than those of pristine VN (55.8%), VN-G-10% (45.3%), VN-G-20% (51.3%), VN-G-50% (51.5%) and graphene reported previously.[27] It was demonstrated that proper mass ratio of VN and G is beneficial to reducing the irreversible capacity. After a few cycles at 21 mAg^{-1}, the reversible capacities of VN, VN-G-10%, VN-G-20%, VN-G-30% and VN-G-50% electrodes are around 140, 130, 240, 280 and 340 mAh g^{-1}, respectively. It also can be found in Fig. 6 that the capacity of

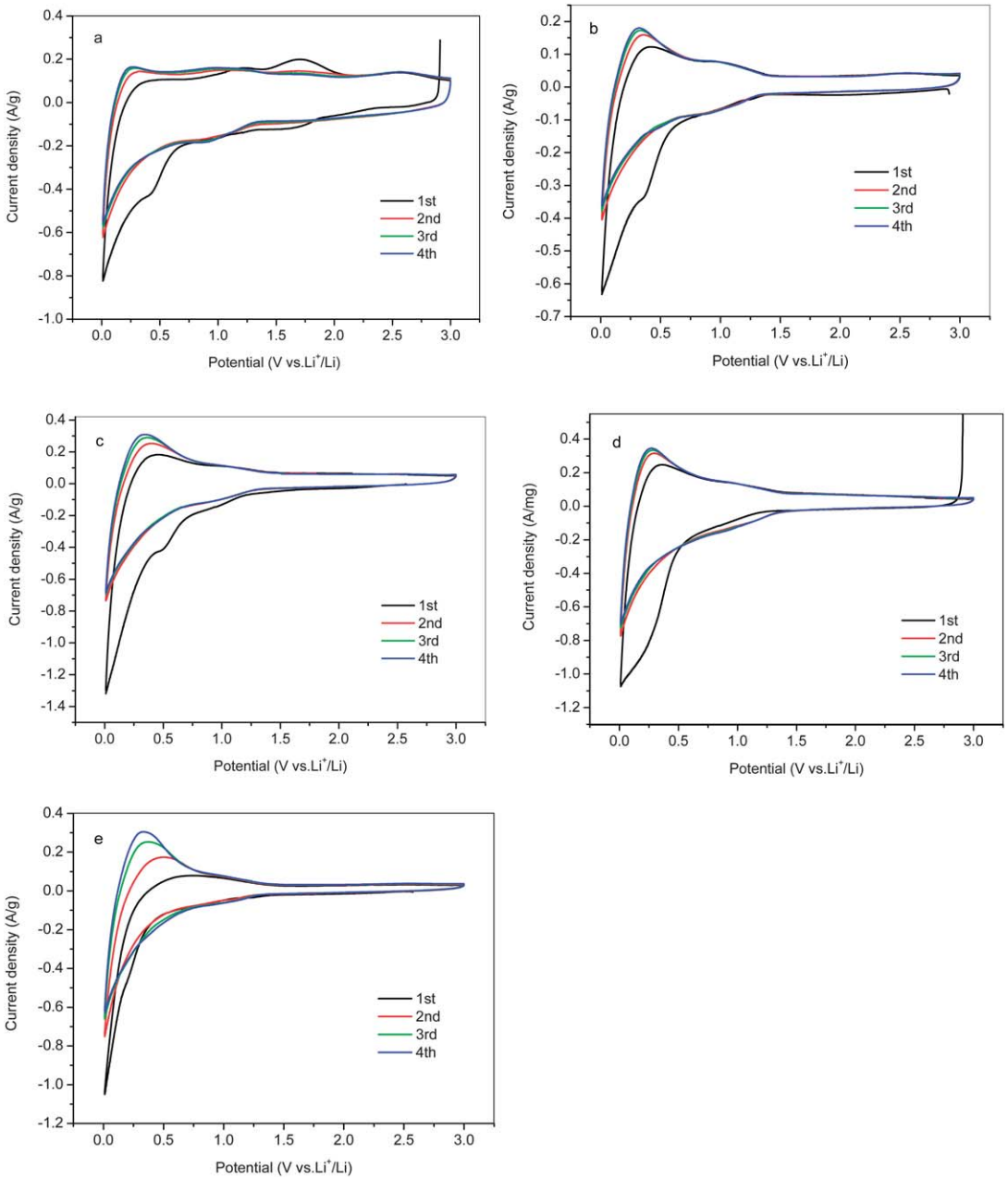

Fig. 4 CV curves of (a) pristine VN, (b) VN-G-10%, (c) VN-G-20%, (d) VN-G-30%, and (e) VN-G-50% electrodes at a scan rate of 1 mV s^{-1} in a potential window from 0.01 to 3.0 V (*vs* Li^+/Li) in EC/DMC solution containing 1 M $LiPF_6$.

VN-G-10% hybrid material is similar to that of pristine VN in cycling performance. This could be ascribed to an un-effective electronic and lithium ion transportation in this hybrid according to the literature reported.[37] When the current densities increased to 42 mA g^{-1}, the reversible capacity of VN-G-50% electrode rapidly drops to 245 mAh g^{-1} and delivers lower capacity than that of VN-G-30% (260 mAh g^{-1}). It is very interesting that when the current density returns to 42 mA g^{-1} after the rate test, the reversible capacity of all the samples was demonstrated to show a significant increase than the original value. For a fair comparison, the bulk VN material had been prepared and tested to possess minor capacity despite a huge capacity of 1500 mAh g^{-1} of thin film VN reported by Fu Z. *et al.*[12] (Fig. S2†). These discrepancies may result from different kinetic and thermodynamic behaviors owing to the so-called size effect, which is analogous to the report by Poizot *et al.* on lithium reacting with transition metal oxides.[38] It was also reported that comparison results between bulk moduli and atomic volumes for the various phases of vanadium nitrides showed that higher bulk moduli are dominated by increased V–N bonds combined with low atomic volumes, which might influence the reaction kinetics of vanadium nitride with lithium.[39] Of course, there is a strong synergistic effect between VN and G after considerable cycles, which was similar to the previous literature.[30] Among them, the specific capacity of VN-G-30% increased to 410 mAh g^{-1} gradually after the rate performance test (Fig. S3†), which is much higher than

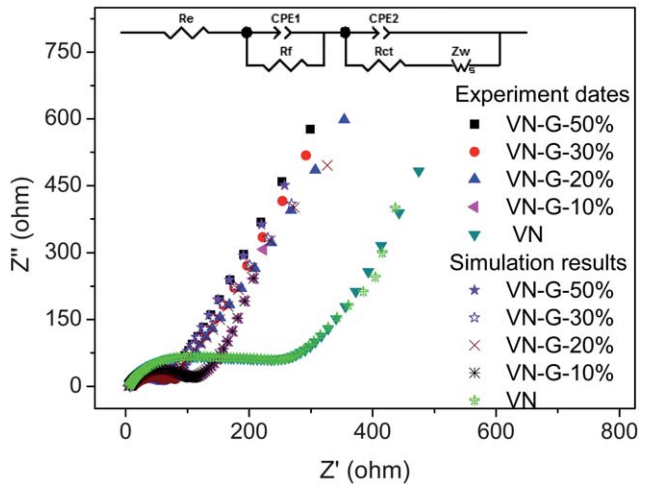

Fig. 5 Nyquist plots of VN-G hybrid and pristine VN electrodes and the corresponding simulation results (inset is the equivalent circuit used to fit an experimental curve).

Table 1 Kinetic parameters of VN-G hybrid materials and pristine VN electrodes

Sample	R_f (Ω)	R_{ct} (Ω)	CPE_1 (F)	CPE_2 (F)
VN	143.6	123.7	1.3×10^{-5}	1.5×10^{-4}
VN-G-10%	109.2	24.1	3.3×10^{-5}	6.7×10^{-4}
VN-G-20%	71.7	22.1	4.7×10^{-5}	1.5×10^{-4}
VN-G-30%	67.8	14.4	5.1×10^{-5}	1.8×10^{-4}
VN-G-50%	60.9	12.9	2.1×10^{-4}	1.4×10^{-5}

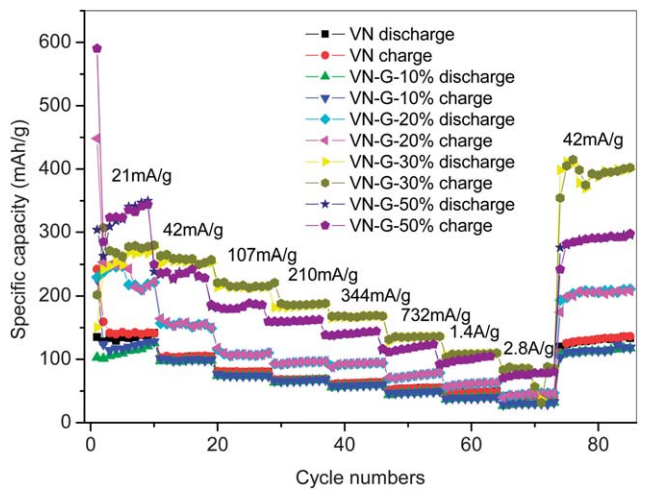

Fig. 6 Cycling and rate performance of VN-G hybrid materials and pristine VN electrodes cycled in EC/DMC solution containing 1 M $LiPF_6$.

other samples. Also its capacity gradually increased to 983 mAh g^{-1} after 175 cycles (Fig. S4†). It might be that VN-G-30% forms a beneficial structure for favourable Li storage as reported by J. Maier *et al.*[40–42] For a fair comparison, a simple mixture of VN and G (7 : 3) was tested under the same experimental conditions. The results showed that the electrochemical performance of the mixture of VN and G (7 : 3) was much worse than VN-G-30% hybrid material (Fig. S5†). The higher capacity of the VN-G hybrid materials is due to the good nanowiring by G.

Investigation using advanced HRTEM, XRD and EELS methods was carried out to elucidate the capacity enhancement mechanism after considerable cycles. It was previously reported by Chen C. *et al.* that the capacity enhancement was originated from one reactive SEI mechanism with a lower columbic efficiency in metal oxides.[43] In our case, the columbic efficiency is almost 100% except for the first few cycles, which is obviously different from the reactive SEI mechanism. XRD patterns after cycle measurement were depicted in Fig. 7. The XRD analyses revealed a shift of electrochemically reformed "VN" peaks towards larger angles (with respect to the initial VN phase) corresponding to a lattice contraction after cycling.[44–46] A possible explanation may be attributed to the formation of a $Li_xV_{1-x}N$ phase as the substitution of Li^+ ions, of about 0.68 Å in diameter, for larger vanadium ions, resulting in a lattice contraction. Note that the absence of Li_3N in the XRD patterns obtained at the end of lithiation is mainly owing to a low atomic scattering factors of its constituents (Li and N), leading to a major difficulty in detection of Li_3N by XRD. In our case, the average diameter of VN particles is larger than 10 nm, as revealed by TEM measurement. Therefore it is highly possible that VN nanoparticles could suffer from a relatively slow kinetics; and more lithium could reversibly reacted with activated nitrides after being activated gradually, which could result in the increasing capacity during cycling. Fig. 8a is a typical bright-field transmission electron micrograph, showing the nanoparticles range from ~15 nm to ~100 nm in diameter. EELS analyses were conducted in two different regions, indicated by "1" and "2" in Fig. 8a, to detect the chemical changes of nitride and vanadium after cycling. Fig. 8b shows the result, with a magnified version of N-K edge shown inset. Normalising the two spectrum using N-K edges gives us a clear clue that the V-L edge is higher in region 1 than that of 2, which implies the content of vanadium is higher in region 1. This leads us to a conclusion that more lithium are

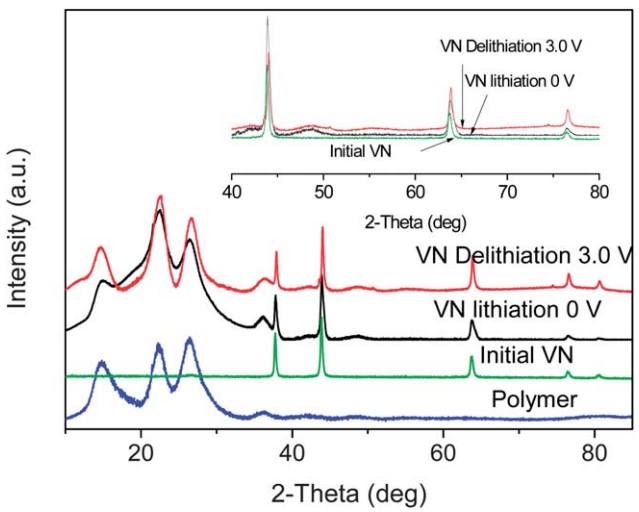

Fig. 7 XRD patterns of the VN electrode obtained at the end of lithiation at 0 V and at the end of delithiation at 3.0 V compared to the initial VN electrode.

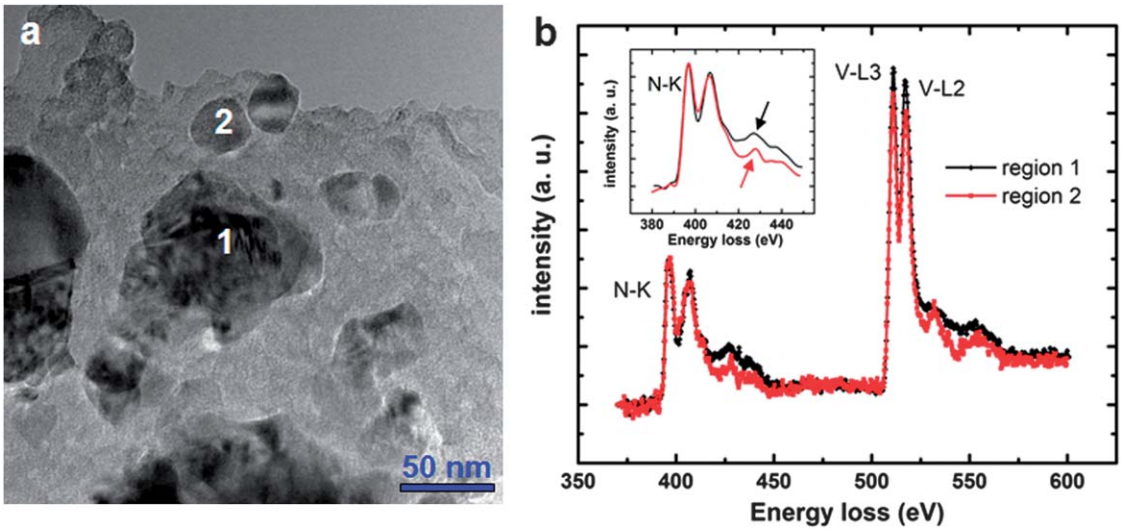

Fig. 8 TEM and EELS analyses of the VN samples after cycles, indicating that lithium ions were incorporated into the vanadium nitride by extended cycling.

incorporated into the lattice by forming Li nitrides in smaller and thinner nanoparticles (region 1). In addition, as indicated by arrows, the extended near-edge fine structure of N-K edge shown inset also displays considerable difference which is closely related to the diffraction conditions of the local structural and chemical environment surrounding nitride atoms, implying the incorporation of lithium ions into the lattice. These results shed light on the fact that for lithium reaction with activated metal nitrides, there may exist a reversible conversion reaction that metal nitrides mainly transform into nanocomposites of metallic M (or MN_{1-x}) + Li_3N, which is analogous to the report by N. Pereira *et al.* on electrochemistry of Cu_3N with lithium.[47] In addition, the increased spacing between the layers of G could provide more active sites for the storage of more lithium, which is similar with carbon nanotube samples reported previously.[48] These results indicate that proper amount of G in the hybrid materials plays a significant role in improving the electrode rate performance and specific capacity owing to the provision of a highly conductive medium for electron transfer during the lithiation and de-lithiation processes.

Conclusions

Preparation of VN-G hybrid with different mass ratios by a sol–gel method followed by heat treatment under ammonia atmosphere is presented. The hybrid material forms an effective conducting network, with VN nanoparticles adhered to and/or embedded in the graphene layers. The electrochemical results clearly demonstrate that there is a strong synergistic effect between VN and G. The hybrid materials exhibited increasing capacity and better rate performance after cycling due to a gradual activation mechanism, which is favorable to the improvement of electrochemical kinetics.

Acknowledgements

We appreciate the support of "100 Talents" program of the Chinese Academy of Sciences, National Program on Key Basic Research Project of China (973 Program) (No. MOST2011CB935700), Shandong Province Fund for Distinguished Young Scientist (BS2009NJ013) and National Natural Science Foundation of China (Grant No. 20971077).

References

1 C. K. Chan, H. Peng, G. Liu, K. McIlwrath and Y. Cui, *Nat. Nanotechnol.*, 2008, **3**, 31–35.
2 J. M. Tarascon and M. Armand, *Nature*, 2001, **414**, 359–367.
3 M. S. Whittingham, *Chem. Rev.*, 2004, **104**, 4271–4302.
4 Y. G. Guo, J. S. Hu and L. J. Wan, *Adv. Mater.*, 2008, **20**, 2878–2887.
5 H. Shi, J. Barker, M. Y. Saidi and R. Koksbang, *J. Electrochem. Soc.*, 1996, **143**, 3466–3472.
6 Y. Idota, T. Kubota, A. Matsufuji, Y. Maekawa and T. Miyasaka, *Science*, 1997, **276**, 1395–1397.
7 K. Amezawa, N. Yamamoto, Y. Tomii and Y. Ito, *J. Electrochem. Soc.*, 1998, **145**, 1986–1993.
8 J. H. Ryu, J. W. Kim, Y. E. Sung and S. M. Oh, *Electrochem. Solid-State Lett.*, 2004, **7**, A306–A309.
9 B. C. Kim, H. Uono, T. Satou, T. Fuse, T. Ishihara, M. Ue and M. Senna, *J. Electrochem. Soc.*, 2005, **152**, A523–A526.
10 I. S. Kim, G. E. Blomgren and P. N. Kumta, *Electrochem. Solid-State Lett.*, 2003, **6**, A157–A161.
11 L. E. Toth, Academic Press Inc., U.S., 1971.
12 Q. Sun and Z. W. Fu, *Electrochim. Acta*, 2008, **54**, 403–409.
13 G. L. Cui, L. Gu, A. Thomas, L. Fu, P. A. van Aken, M. Antonietti and J. Maier, *ChemPhysChem*, 2010, **11**, 3219–3223.
14 K. S. Novoselov, A. K. Geim, S. V. Morozov, D. Jiang, Y. Zhang, S. V. Dubonos, I. V. Grigorieva and A. A. Firsov, *Science*, 2004, **306**, 666–669.
15 J. Yan, Z. Fan, T. Wei, W. Qian, M. Zhang and F. Wei, *Carbon*, 2010, **48**, 3825–3833.
16 L. P. Ma, Z. S. Wu, J. Li, E. D. Wu, W. C. Ren and H. Cheng, *Int. J. Hydrogen Energy*, 2009, **34**, 2329–2332.
17 N. A. Kaskhedikar and J. Maier, *Adv. Mater.*, 2009, **21**, 2664–2680.
18 C. Soldano, A. Mahmood and E. Dujardin, *Carbon*, 2010, **48**, 2127–2150.
19 C. G. Lee, X. D. Wei, J. W. Kysar and J. Hone, *Science*, 2008, **321**, 385–388.
20 A. Rouhanipour, M. Roy, X. L. Feng, H. J. Räder and K. Müllen, *Angew. Chem., Int. Ed.*, 2009, **48**, 4602–4604.
21 A. A. Balandin, S. Ghosh, W. Bao, I. Calizo, D. Teweldebrhan, F. Miao and C. N. Lau, *Nano Lett.*, 2008, **8**, 902–907.
22 Y. Y. Liang, D. Q. Wu, X. L. Feng and K. Müllen, *Adv. Mater.*, 2009, **21**, 1679–1683.

23 G. Wang, X. Shen, J. Yao and J. Park, *Carbon*, 2009, **47**, 2049–2053.
24 G. Wang, B. Wang, X. Wang, J. Park, S. Dou, H. Ahn and K. Kim, *J. Mater. Chem.*, 2009, **19**, 8378–8384.
25 S. M. Paek, E. J. Yoo and I. Honma, *Nano Lett.*, 2008, **9**, 72–75.
26 D. Wang, D. Choi, J. Li, Z. Yang, Z. Nie, R. Kou, D. Hu, C. Wang, L. V. Saraf, J. Zhang, I. A. Aksay and J. Liu, *ACS Nano*, 2009, **3**, 907–914.
27 H. B. Wang, Z. H. Liu, L. Wang, P. H. Han and G. L. Cui, *J. Mater. Chem.*, 2011, **21**, 5430–5434.
28 W. S. Hummers and R. E. Offeman, *J. Am. Chem. Soc.*, 1958, **80**, 1339–1339.
29 A. M. Glushenkov, D. Hulicova-Jurcakova, D. Llewellyn, G. Q. Lu and Y. Chen, *Chem. Mater.*, 2010, **22**, 914–921.
30 Z. S. Wu, W. Ren, L. Wen, L. Gao, J. Zhao, Z. Chen, G. Zhou, F. Li and H. M. Cheng, *ACS Nano*, 2010, **4**, 3187–3194.
31 C. Xu, X. Wang, L. C. Yang and Y. P. Wu, *J. Solid State Chem.*, 2009, **182**, 2486–2490.
32 J. Yao, X. Shen, B. Wang, H. Liu and G. Wang, *Electrochem. Commun.*, 2009, **11**, 1849–1852.
33 R. Alcantara, P. Lavela, G. F. Ortiz, J. L. Tirado, E. Zhecheva and R. Stoyanova, *J. Electrochem. Soc.*, 2007, **154**, A964–A970.
34 Z. W. Fu, Y. Wang, X.-L. Yue, S.-L. Zhao and Q.-Z. Qin, *J. Phys. Chem. B*, 2004, **108**, 2236–2244.
35 A. Rouhanipour, M. Roy, X. L. Feng, H. J. Räder and K. Müllen, *Angew. Chem., Int. Ed.*, 2009, **48**, 4602–4604.
36 Y. G. Guo, J. S. Hu and L. J. Wan, *Adv. Mater.*, 2008, **20**, 2878–2887.
37 H. L. Wang, L. F. Cui, Y. Yang, J. T. Robinson, Y. Cui and H. J. Dai, *J. Am. Chem. Soc.*, 2010, **132**, 13978–13980.
38 P. Poizot, S. Laruelle, S. Grugeon, L. Dupont and J. M. Tarascon, *Nature*, 2000, **407**, 496–501.
39 C. Ravi, H. K. Sahu and M. C. Valsakumar, *Phys. Rev. B.*, 2010, **81**, 104–111.
40 J. Maier, *Nat. Mater.*, 2005, **4**, 805–809.
41 P. Balaya, H. Li, L. Kienie and J. Maier, *Adv. Mater.*, 2006, **18**, 1421–1427.
42 J. Jamnik and J. Maier, *Phys. Chem. Chem. Phys.*, 2003, **5**, 5215–5220.
43 C. Chen and Z. W. Wang, *Commun. Theor. Phys.*, 2005, **43**, 305.
44 N. Pereira, M. Balasubramanian, L. Dupont and G. G. Amatucci, *J. Electrochem. Soc.*, 2003, **150**, A1118–A1128.
45 Z. W. Zhang, C. G. Hu, Y. F. Xiong and Z. L. Wang, *Nanotechnology*, 2007, **18**, 465504–465509.
46 B. Winkler, A. Erick, J. Arellano, A. Friedrich and J. Y. Yan, *Solid State Sci.*, 2010, **12**, 2059–2064.
47 N. Pereira, L. Dupont, J. M. Tarascon, L. C. Klein and G. G. Amatucci, *J. Electrochem. Soc.*, 2003, **150**, A1273–A1280.
48 N. A. Kaskhedikar and J. Maier, *Adv. Mater.*, 2009, **21**, 2664–2680.

